ACS OMEGA

http://pubs.acs.org/journal/acsodf

Article

Magnetically Separable Visible Light-Active $Ag_{0.75}Ni_{0.25}$ Binary Alloy Nanoparticles as a Highly Efficient Photocatalyst for the Selective Oxidative Coupling of Aniline to Azobenzene

Soniya Agarwal, Bidisa Dowara, Sanjeev Kumar, Vinod Kumar, and Kalyanjyoti Deori*

Cite This: *ACS Omega* 2022, 7, 48615−48622

Read Online

ACCESS | Metrics & More | Article Recommendations | Supporting Information

ABSTRACT: Aniline wastes can be converted to useful pharmaceutical and industrial compounds like azobenzene. For this purpose, a bimetallic $Ag_{0.75}Ni_{0.25}$ alloy is designed in the nanoscale range resembling a fivefold twinned morphology using water as the solvent. These newly developed alloy nanoparticles (NPs) are employed for the first time as an efficient visible light-active photocatalyst for the oxidative homocoupling of aniline to azobenzene. Our catalytic protocol is highly sustainable for a large number of aniline substrates with a high yield of the product (up to 95%), which might be attributed to the combinational and superior properties achieved on alloy formation in comparison to the monometallic counterparts. High-electron density amines (p-anisidine) display greater photocatalytic proficiency than that of low-electron density amines (4-fluoroaniline). The developed photocatalyst is magnetically well-separable and can be reused for at least five catalytic cycles without appreciable loss in its activity.

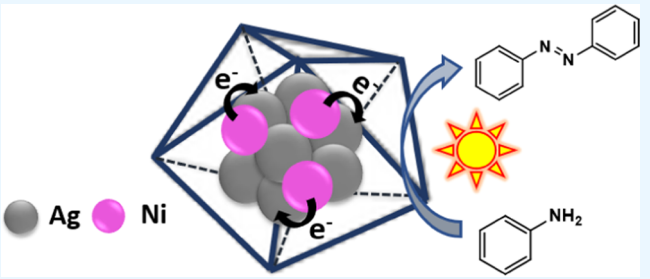

INTRODUCTION

Use of green and renewable energy sources in industrially important catalytic processes is considered a viable alternative for traditional thermal energy, as the former is in general more amiable, greener, and inexpensive. Being one of the most abundant and clean energy sources, use of visible light is therefore undoubtedly more attractive and safer for various organic transformations to prepare value-added chemicals.[1,2] Aromatic azo compounds are such important chemicals that have been a subject of interest among organic chemists because of their diverse potential applications in the industrial sector as dyes, pigments, medicinal scaffolds, radical initiators, indicators, and food additives.[3−5] They also serve as building blocks to various polymers and natural products.[6] Due to their widespread application, many reports are available for the synthesis of azo compounds and their derivatives involving different approaches and strategies such as diazotization of anilines,[7] oxidative coupling of anilines,[8,9] reduction of azoxybenzenes,[4] and reductive coupling of nitro aromatics.[10] Among these, oxidative coupling of anilines is a straight forward and recognized synthetic route in the scientific community, which involves the use of an oxidizing agent such as Mn-based reagents,[11] $Pb(OAc)_4$,[12] *tert*-butyl hypoiodite, and HgO. Although many protocols with metal catalysts (MnOOH nanotubes,[13] Ru_xPd_y@rGO alloy nanoparticles (NP),[14] AuAg alloy NP,[15] Ag NP,[16] AgNi alloy NP,[17] Cu_2O-RuO_2,[18] Cu(0),[19] $PdCl_2$-$Cu(OAc)_2$[20]) have been introduced using air or O_2 as an oxidant, they usually involve high temperature and long reaction time. Very few studies report the synthesis of azobenzene using a renewable energy source, i.e., visible light irradiation with high selectivity toward azobenzene.[21−23]

Among the recently reported catalysts, for the aforesaid synthesis, majority is covered by bimetallic alloy NPs.[14,15,17] Alloy NPs are emerging as a potential catalyst for the discussed and many other organic transformations such as nitro reduction, alcohol oxidation, CO oxidation, electrochemical ethanol and methanol oxidation, furfural hydrogenation, and degradation of organic pollutants.[24,25] A bimetallic nanoalloy offers unique magnetic, electronic, and catalytic properties and displays composition-dependent activity.[26] The unification of one transition metal with a noble metal crafts a cost-effective potential photocatalyst, and studies suggest that AgNi can best serve for this purpose.[27,28] However, the lower surface energy offered by Ag, 14% lattice mismatch, complete immiscibility, and greater difference in reduction potential between the metals Ag and Ni make the synthesis of the alloy difficult and prefer a thermodynamically favorable core@shell structure.[29,30] At the nanoscale, these restrictions can however be minimized

Received: November 20, 2022
Accepted: December 2, 2022
Published: December 12, 2022

for alloy formation due to surface defects.[31] Many techniques such as radiolysis,[32] thermal decomposition,[33] and chemical reduction[34] are reported by various groups for the synthesis of bimetallic AgNi alloys. Kumar et al. reported the synthesis of AgNi alloy NPs as a catalyst for azobenzene production, but the work has certain drawbacks.[17] First, the alloy was synthesized by the assistance of the organic surfactants hexadecylamine and 1-octadecene at a high reaction temperature of 250 °C, and second, the oxidative coupling of aniline to azobenzene was performed under thermal conditions. In this report, we have developed a novel hydrothermal route to synthesize a nanostructured binary $Ag_{0.75}Ni_{0.25}$ alloy with fivefold twinned morphology and explored it for the first time as one of the most efficient and potential visible light-active photocatalysts for the synthesis of a variety of aromatic azo compounds. We refurbished the catalytic protocol using mild reaction conditions and a greener energy source for the selective oxidative homocoupling of aniline. The synthesized catalyst is magnetically separable and can be reused for five consecutive cycles without any substantial loss in the activity.

EXPERIMENTAL SECTION

Chemicals and Reagents. Silver nitrate ($AgNO_3$, SRL, 99.5%), nickel chloride hexahydrate ($NiCl_2{\cdot}6H_2O$, SRL, 99%), cetyltrimethylammonium bromide (CTAB, Spectrochem, 98%), hydrazine hydrate ($N_2H_4{\cdot}H_2O$, Spectrochem, 80%), potassium hydroxide (KOH, Qualigens, 85%), acetonitrile (ACN, Spectrochem, 99%), and aniline and related substrates (TCI, >98%) were used.

Synthesis of AgNi Alloy Nanoparticles. AgNi alloy NPs were synthesized by developing a novel protocol following the hydrothermal route. In the synthetic protocol, 0.5 mmol $NiCl_2{\cdot}6H_2O$, 0.5 mmol $AgNO_3$, and 3 mmol CTAB were dissolved in 20 mL of deionized H_2O by stirring for 10 min and further sonicating it for 30 min. After obtaining a homogeneous mixture, 15 mL of a mixture of 0.5 M NaOH and $N_2H_4{\cdot}H_2O$ in 1:1 ratio was added dropwise and a black precipitate was obtained. The whole solution was then transferred to an autoclave and treated at 150 °C for 6 h. After attaining room temperature, it was collected via a magnet and washed with ethanol four times and dried to obtain 111 mg and named as $Ag_{0.5}Ni_{0.5}$. In a similar manner, a AgNi alloy with a different precursor ratio of 3:1 was named as $Ag_{0.75}Ni_{0.25}$ with 120 mg of the end product and that with 1:3 was named as $Ag_{0.25}Ni_{0.75}$ and a 103 mg sample was collected.

Two more samples were synthesized following the same procedure, first by omitting Ni salt and the other by omitting Ag salt, named as Ag-1 and Ni-1, respectively.

Characterization of AgNi Alloy Nanoparticles. The powder X-ray diffraction (PXRD) pattern of the as-synthesized samples was obtained with a Bruker D8 Advance X-ray diffractometer by treating monochromatic Cu Kα radiation (λ = 1.54056 Å). X-ray photoelectron spectroscopy (XPS) measurements were done using a PHI 5000 Versa Probe III instrument. All the obtained binding energy data were calibrated with reference to the C 1s (284.6 eV) peak. Transmission electron microscopy (TEM) images, high-resolution TEM (HR-TEM) images, and selected-area electron diffraction patterns (SAED) were attained with a Technai transmission electron microscope functioning at 200 kV armed with digital imaging and 35 mm photography systems. Inductively coupled plasma mass spectrometry (ICP-MS) analysis was carried out on a Thermo Fischer iCAP RQ ICP-MS. The magnetic data were obtained from a Lakeshore model 7400 series vibrating sample magnetometer (VSM). UV–visible absorption patterns were obtained from a Shimadzu UV-1700 UV-Vis spectrophotometer. A Bruker Ascend 500 MHz spectrophotometer was used to obtain ^1H and ^{13}C nuclear magnetic resonance (NMR) spectra at 500 and 125 MHz, respectively.

General Synthetic Route for Photocatalytic Oxidative Coupling of Aniline to Azobenzene. In a typical photocatalytic reaction for the synthesis of azobenzene, 0.5 mmol aniline was taken in a reaction tube and to it, 1 mmol KOH and 5 mg of the as-synthesized photocatalyst AgNi were added. To this reaction mixture, 1 mL of acetonitrile (ACN) was added as the solvent and at last, 1 mL of 30% H_2O_2 was added as the oxidizing agent. The reaction mixture was then stirred with continuous irradiation of visible light. Once the TLC showed complete conversion, the product was extracted in diethyl ether and washed with 0.1 N HCl solution to convert any unreacted aniline to its corresponding salt for easy separation of the unreacted aniline substrate, and next, column chromatography was done to obtain the purified product. Finally, the extract was reduced under high pressure and characterized by ^1H and ^{13}C NMR spectra.

The photocatalytic reactions were carried out in a photocatalytic reactor equipped with a 250 W (210.4 lux) visible light source permitting a wavelength distribution of 400–700 nm at a distance of 6 cm from the reaction tubes placed on a magnetic stirrer. Moreover, the temperature within the range of 27–30 °C was maintained via a cold-water circulating tank attached to the reaction chamber.

RESULTS AND DISCUSSION

Three samples of bimetallic AgNi alloy NPs with different molar ratios of Ag and Ni were synthesized by developing a hydrothermal protocol following the principle of coreduction in aqueous medium. The three as-synthesized samples were initially probed for phase purity and composition by obtaining the PXRD patterns (Figure 1). Interesting observations were

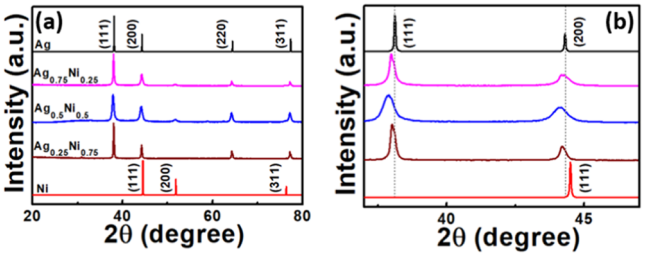

Figure 1. (a) PXRD pattern of the as-synthesized AgNi alloy NPs and standard pattern of Ag and Ni and (b) magnified view of (a) from 37 to 47°.

concluded from the attained PXRD patterns. The patterns revealed the formation of a *fcc* lattice resembling the (111), (200), (220), and (311) planes of Ag with slight deviation from the respective 2θ values of 38.11, 44.32, 64.42, and 77.47°. The higher reduction potential of Ag (Ag^+/Ag, 0.80 V) than that of Ni (Ni^{2+}/Ni, −0.25 V) favors the formation of the Ag matrix and occupation of the lattice sites by Ni after its successive reduction, and hence, peaks resembling only the Ag lattice are observed. The absence of individual peaks from the PXRD pattern revealed the formation of an alloy sample. As

https://doi.org/10.1021/acsomega.2c07441
ACS Omega 2022, 7, 48615–48622

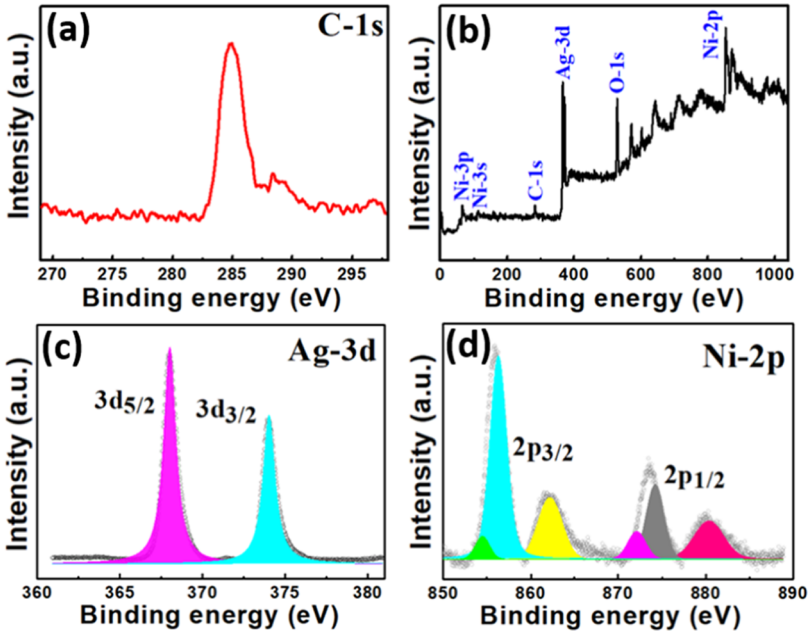

Figure 2. (a) XPS spectra of C 1s and (b) wide survey scan and high-resolution XPS spectra of (c) Ag 3d and (d) Ni 2p of $Ag_{0.75}Ni_{0.25}$ alloy NPs.

the concentration of Ni increases in the alloy samples, all the peaks shift toward right, i.e., to a higher diffraction angle (Figure 1b). This is due to the occupation of the Ag (144 pm) lattice sites by the smaller Ni (124 pm) atoms, which also results in the overall decrease in the value of lattice constant and the formation of a homogeneous solid solution-type alloy, which is also supported by Vegard's law. According to Vegard's law

$$a(Ag_{0.75}Ni_{0.25}) = 0.75a(Ag) + 0.25a(Ni)$$

where $a(Ag_{0.75}Ni_{0.25})$ is the lattice constant for the bimetallic alloy sample $Ag_{0.75}Ni_{0.25}$ and $a(Ag)$ and $a(Ni)$ are the lattice constants for the constituents Ag and Ni, respectively. On calculation from the PXRD data, we get

$$a(Ag_{0.75}Ni_{0.25}) = 4.09675$$

$$0.75a(Ag) + 0.25a(Ni) = 3.94562$$

hence satisfying Vegard's law and proving the formation of alloy.

The data obtained by ICP-MS analysis of the alloy samples revealed the elemental composition consistent with the initial feed ratio (Table S1).

The elemental composition along with the valence state of Ag and Ni in the as-synthesized alloy sample was further confirmed by XPS measurements. The XPS spectra of C 1s (Figure 2a) were calibrated to a binding energy value of 284.6 eV. The survey scan spectrum (Figure 2b) reveals the presence of Ag and Ni as the main elements of the alloy sample with a small amount of C and O, which might be due to the bound CTAB or surface oxidation of the alloy sample. The XPS spectra of Ag show two peaks for the 3d core at 367.9 eV (Ag $3d_{5/2}$) and 373.9 eV (Ag $3d_{3/2}$) corresponding to metallic Ag (Figure 2c), whereas the peaks for Ni $2p_{3/2}$ and Ni $2p_{1/2}$ appear at 856.2 and 874.5 eV, respectively, with satellite peaks at 861.8 and 879.8 eV, indicating Ni in the +2 valence state due to surface oxidation. Peaks at 854.1 and 871.8 eV correspond to the zero valence state of Ni (Figure 2d). All the data obtained for surface oxidation states are in complete agreement with the reported literature values, approving nanoalloy formation.[35,36]

Ascertaining the elemental composition, the alloy sample was probed for size and morphology by TEM and HR-TEM analysis. The incorporation of Ni into the Ag matrix gave particles in the range of 20−60 nm as observed in the TEM image (Figure 3a) of the $Ag_{0.75}Ni_{0.25}$ nanoalloy. On magnifying a single particle, the HR-TEM image displays the formation of a fivefold intertwined geometry resembling a decahedral morphology (Figure 3b). The *fcc* Ag thermodynamically favors the fivefold twinning so as to lower the surface energy. The lattice spacing on the faces of the twinned morphology is 0.203 nm, resembling the (200) plane of the AgNi alloy (Figure 3c).

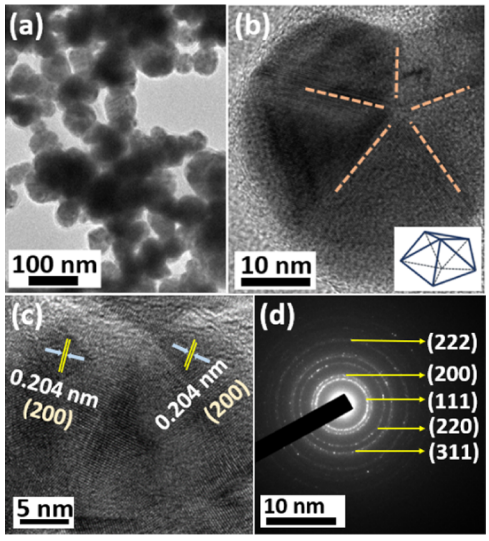

Figure 3. (a) TEM image; (b) and (c) HR-TEM image; and (d) SAED pattern STEM image; and elemental mapping for the constituent elements (e) Ag and Ni, (f) Ag, and (g) Ni of the as-synthesized $Ag_{0.75}Ni_{0.25}$ alloy NPs.

https://doi.org/10.1021/acsomega.2c07441
ACS Omega 2022, 7, 48615−48622

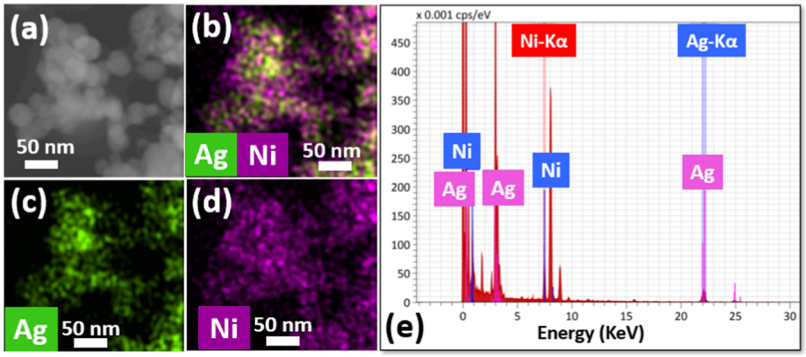

Figure 4. (a) STEM image and elemental mapping for the constituent elements (b) Ag and Ni, (c) Ag, and (d) Ni and (e) TEM-EDS spectra of the as-synthesized $Ag_{0.75}Ni_{0.25}$ alloy NPs.

The *d*-spacing values (Table S2) for all the constituent crystal planes were calculated from the SAED pattern (Figure 3d), and they show an increase from the standard values, in approval with the PXRD pattern. An important criterion for alloy formation is the identification of homogeneous distribution of the compositional elements within the particle. Elemental mapping in the STEM mode of the NPs shows uniform distribution and superimposition of both the constituent elements, omitting the possibility of the formation of any core−shell structure or phase separation (Figure 4). All the obtained data clearly indicate an alloy formation from the designed synthetic protocol. The elemental ratio (Ag:Ni) obtained from the TEM-energy dispersive spectroscopy (TEM-EDS) spectra (Figure 4e) is in complete agreement with the ICP-MS data (Table S1).

Alloying of Ni with Ag led us to test the magnetic properties of the nanosized sample. The magnetic hysteresis curve of $Ag_{0.75}Ni_{0.25}$ alloy NPs (Figure 5) derived a coercivity value of

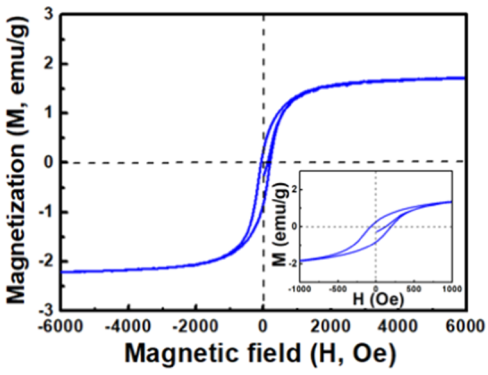

Figure 5. Magnetic hysteresis curve of the as-synthesized $Ag_{0.75}Ni_{0.25}$ alloy NPs (inset: magnified curve).

132.5 Oe, remanent magnetization equal to 0.538 emu/g, and saturation magnetization equal to 2.063 emu/g. The measured magnetic parameters denote the synthesis of a weak ferromagnetic sample and hence unfolds many potential applications.

The incorporated noble Ag metal has the ability to show strong resonance in the absorption spectra depending upon the particle shape, size, and environment. Therefore, the UV−visible spectra of the as-synthesized $Ag_{0.75}Ni_{0.25}$ alloy were probed and a broad absorption in the near-visible and visible regions was observed. (Figure S1).

Photocatalytic oxidative coupling of aniline to azobenzene was chosen as the test reaction to test the proficiency of the as-synthesized samples. Before testing the photocatalytic activity, the reaction was optimized according to the popular reported conditions, i.e., DMSO as the solvent and KOH as the base at 60 °C in air with aniline as the substrate. First, the reaction was done without the supply of heat or light (Table S3, entry 1) with the as-synthesized $Ag_{0.5}Ni_{0.5}$ alloy as the catalyst, and no product formation was observed. On heating the reaction mixture at 60 °C (Table S3, entry 2), the product was obtained with 72% yield. The other two synthesized ratios of the alloy ($Ag_{0.75}Ni_{0.25}$ and $Ag_{0.25}Ni_{0.75}$) were also checked for catalytic efficiency (Table S3, entry 3 and 4), and as anticipated, $Ag_{0.75}Ni_{0.25}$ gave the product with the highest yield, and hence, further optimization was proceeded with $Ag_{0.75}Ni_{0.25}$ alloy NPs. Accordingly, the optimized conditions were found to be 5 mg of $Ag_{0.75}Ni_{0.25}$, 0.5 mL of DMSO, and 1 mmol KOH at 60 °C with air as the oxidant for 91% product yield in 5 h (Table S3, entry 6). Moving toward a greener route, we replaced heat as the activation source with light. No product was initially formed (Table S4, entry 1), but by replacing the solvent with acetonitrile and adding H_2O_2 as the oxidizing agent, the product was obtained in quantitative yield (Table S4, entry 3 and 4). Few more reactions were done to check the effect of the amount of the solvent, base, and light (Table S4, entry 2, 5, 6, 7, 8, and 9). Moreover, to ensure the efficiency and activity of our photocatalyst and to establish the importance of nanoalloy synthesis as an industrially significant catalyst, oxidative coupling of aniline was carried out with Ag-1, Ni-1, $AgNO_3$, and $NiCl_2{\cdot}6H_2O$ (Figure S2), but in no case, a satisfactory yield of azobenzene was achieved. In no case, neither any overoxidized azo products like azoxybenzene nor nitrobenzene formation was observed. The amalgamation of Ag with Ni not just reduces the cost of the expensive noble metal catalyst but also makes the material UV−visible-active due to its inherent property of surface plasmon resonance.

Based on our final optimized conditions, in continuous irradiation of 250 W visible light, an array of substituted anilines was studied for the corresponding azobenzene production. Oxidative coupling progressed smoothly for both electron-withdrawing and electron-donating substituents, furnishing a measurable yield (Table 1). We have incorporated the study on the effect of both electron-donating and electron-withdrawing substituents such as $-CH_3$, $-OCH_3$, −Cl, −Br, −I, $-NH_2$, and $-NO_2$, placed variedly in ortho, meta, and para positions. A high yield of the product was obtained when the electron-donating group was present at the para position, but

https://doi.org/10.1021/acsomega.2c07441
ACS Omega 2022, 7, 48615−48622

Table 1. Substrate Scope for the $Ag_{0.75}Ni_{0.25}$ Photocatalyzed Oxidative Coupling of Aryl Amines[a]

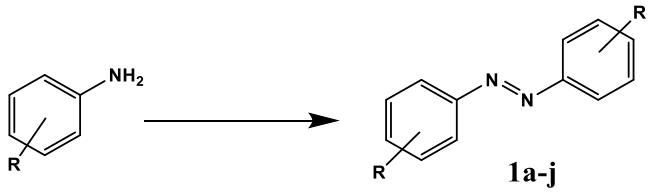

Entry	Substrate	Product	Time (h)	Isolated yield (%)
1	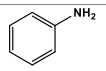	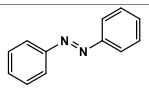	4	92
2	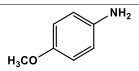	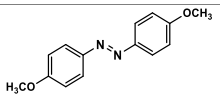	3.5	95
3	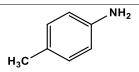	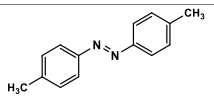	7	66
4	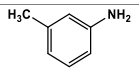	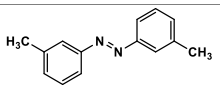	5	87
5	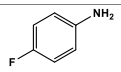	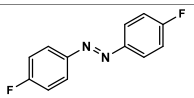	6	71
6	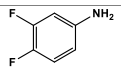	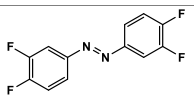	6	67
7	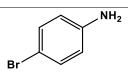	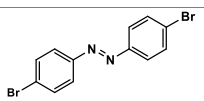	4	82
8	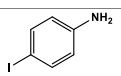	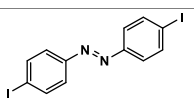	6	80
9		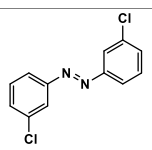	6	86
10	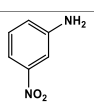	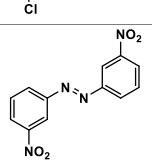	6	87
11	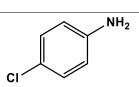	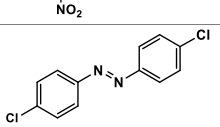	6	75
12	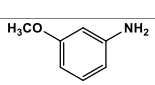	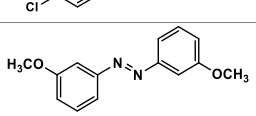	4	91
13	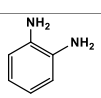	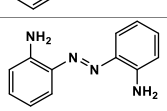	6	88

[a]Reaction conditions: aryl amine (0.5 mmol), $Ag_{0.75}Ni_{0.25}$ (5 mg), KOH (1 mmol), ACN (1 ml), and 30% H_2O_2 (1 ml) at room temperature.

https://doi.org/10.1021/acsomega.2c07441
ACS Omega 2022, 7, 48615−48622

the yield decreases from 95% to 91% upon meta-substitution (Table 1, entry 2, 12). Electron-donating groups at the para position increase the electron density around the $-NH_2$ group, which facilitates easy proton removal necessary for the next step of the coupling reaction. To check the behavior of an aniline substrate toward oxidative coupling if an amine group is present, one new substrate benzene-1,2-diamine is subjected to the catalytic test and it was found that (*E*)-2,2′-(diazene-1,2-diyl)dianiline (Table 1, entry 13) is the major product formed. The reason for this monosubstitution or the coupling to only one amine group is the steric hindrance due to the presence of other $-NH_2$ groups. The coupling to the other amine is restricted after the first, and hence, (*E*)-2,2′-(diazene-1,2-diyl)dianiline was formed as the major product.

The synthesis of azobenzene as the sole product was first ascertained by Fourier transform infrared spectroscopy (FT-IR) analysis (Figure S5), where a characteristic peak for the −N═N− stretching vibration appears at 1586 cm^{-1} and no absorption for N−H was observed. Also, the product formation was confirmed by ^1H and ^{13}C NMR spectra (Figures S6−S9).

This developed photocatalytic protocol for oxidative coupling of aniline to azobenzene is very much efficient, greener, and economic in comparison to most of the recently reported studies (Table S5). A plausible photocatalytic mechanism is proposed based on the obtained evidence and study of the available reported literature in Figure 6.

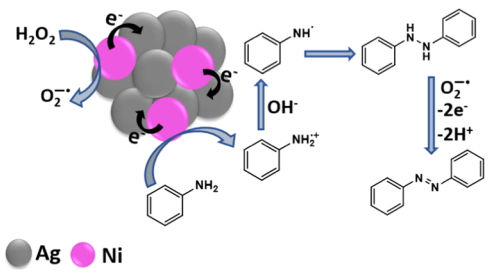

Figure 6. Proposed mechanism for the photocatalytic oxidative coupling of aniline to azobenzene.

Controlled catalytic reactions with Ag-1 and Ni-1 (Figure S2) as the catalysts establish the high activity of Ag over Ni. Moreover, the excellent activity of $Ag_{0.75}Ni_{0.25}$ compared to that of an individual constituent metal also suggests the contribution of the synergy between the metals toward oxidative coupling of aniline to azobenzene. The electronegativity difference between Ag (1.93) and Ni (1.91) facilitates electron transfer from Ni to Ag and creates electron-deficient and electron-rich sites. In addition, the high content of Ag in the alloy offers surface plasmon resonance for prolonged charge separation and increased visible light sensitivity. These electron-deficient sites serve as the driving force of the reaction by generating $O_2^{-\bullet}$ from H_2O_2 along with amine free radicals with the assistance of the base (KOH) by proton abstraction. As a result of radical coupling between the amine radicals, a N−N bond is formed to give a hydrazobenzene intermediate, and then, further oxidation of the intermediate yields the desired azo product.[21,35,37]

The sustainability of any catalyst is determined by its ability to surpass the recyclability test. Aniline was opted as the model substrate to investigate the reutilization of the photocatalyst for the oxidative coupling. The photocatalyst after one reaction cycle was recollected using a magnet, and about 96% of this used photocatalyst was successfully recovered to be used for the next cycle. The recovered sample was washed with deionized water and ethanol and dried and again employed in the next catalytic cycle. In this manner, the photocatalyst was recycled for five consecutive cycles, and a small decline in the product yield was observed only from the third cycle (Figure S3). The justification for the activity retentivity of the catalyst and the minute but gradual decrease in the product yield was obtained by the PXRD pattern (Figure S4a) and TEM image (Figure S4b,c) of the reused catalyst. Both the analyses display characteristics similar to those of the fresh sample along with the presence of two new peaks in between 40 and 50° in the PXRD pattern (Figure S4a), which may be attributed to the slight surface oxidation of alloy NPs after repeated catalytic cycles.

CONCLUSIONS

In summary, we have designed AgNi alloy NPs resembling a decahedral-type morphology with varying compositions of Ag and Ni without the use of any expensive organic surfactant using a novel hydrothermal protocol. The amalgamation of both the constituent metals was confirmed by PXRD, XPS, TEM, and HR-TEM analyses. Out of all the compositions of the prepared alloys, $Ag_{0.75}Ni_{0.25}$ alloy NPs efficiently catalyzed the oxidative homocoupling of aniline to azobenzene on irradiation of visible light, presenting a greener approach for the synthesis of industrially important compounds. By employing a renewable energy source and H_2O_2 as a environmentally benign oxidant, a successful approach for azobenzene production is put forward. After the catalytic reaction, AgNi alloy NPs can be recovered magnetically and reused for five consecutive cycles without any substantial loss in the activity.

ASSOCIATED CONTENT

Supporting Information

The Supporting Information is available free of charge at https://pubs.acs.org/doi/10.1021/acsomega.2c07441.

ICP-MS data; *d*-spacing calculation; optimization table for oxidative coupling of azobenzene; PXRD pattern and TEM images of the recycled catalyst; and ^1H and ^{13}C NMR spectra (PDF)

AUTHOR INFORMATION

Corresponding Author

Kalyanjyoti Deori − *Department of Chemistry, Dibrugarh University, Dibrugarh 786004 Assam, India;* orcid.org/0000-0003-0411-8324; Email: kalchemdu@gmail.com, kalchemdu@dibru.ac.in

Authors

Soniya Agarwal − *Department of Chemistry, Dibrugarh University, Dibrugarh 786004 Assam, India;* orcid.org/0000-0002-3257-6501

Bidisa Dowara − *Department of Chemistry, Dibrugarh University, Dibrugarh 786004 Assam, India*

Sanjeev Kumar − *Department of Chemistry, University of Delhi, Delhi 110007, India*

Vinod Kumar − *Department of Chemistry, University of Delhi, Delhi 110007, India; Special Centre for Nano Sciences,*

https://doi.org/10.1021/acsomega.2c07441
ACS Omega 2022, 7, 48615−48622

Jawaharlal Nehru University, Delhi 110067, India;
orcid.org/0000-0002-8362-8009

Complete contact information is available at:
https://pubs.acs.org/10.1021/acsomega.2c07441

Notes

The authors declare no competing financial interest.

■ ACKNOWLEDGMENTS

S.A. is grateful to the SERB, India, for research fellowship. K.D. is thankful to SERB-DST, India (Grant EEQ/2018/000326), for financial support. The authors are thankful to Dibrugarh University for providing infrastructural facility. The authors also acknowledge IISER Mohali for TEM analysis, IIT Kanpur for XPS analysis, IIT Guwahati for VSM data, and CSIC Dibrugarh University for NMR measurements.

■ REFERENCES

(1) Agarwal, S.; Phukan, P.; Sarma, D.; Deori, K. Versatile precursor-dependent copper sulfide nanoparticles as a multifunctional catalyst for the photocatalytic removal of water pollutants and the synthesis of aromatic aldehydes and NH-triazoles. *Nanoscale Adv.* **2021**, *3*, 3954−3966.

(2) Agarwal, S.; Deori, K. Copper sulfide nanosheets for photocatalytic oxidation of benzyl alcohols and hydroxylation of arylboronic acids. *ACS Appl. Nano Mater.* **2022**, *5*, 4413−4422.

(3) Simplício, A. L.; Clancy, J. M.; Gilmer, J. F. Prodrugs for amines. *Molecules* **2008**, *13*, 519−547.

(4) Merino, E. Synthesis of azobenzenes: the coloured pieces of molecular materials. *Chem. Soc. Rev.* **2011**, *40*, 3835−3853.

(5) Bhardwaj, V. K.; Singh, N.; Hundal, M. S.; Hundal, G. Mesitylene based azo-coupled chromogenic tripodal receptors—a visual detection of Ag (I) in aqueous medium. *Tetrahedron* **2006**, *62*, 7878−7886.

(6) Zhou, Q.; Fursule, I.; Berron, B. J.; Beck, M. J. Toward spatiotemporally controlled synthesis of photoresponsive polymers: computational design of azobenzene-containing monomers for light-mediated ROMP. *J. Phys. Chem. A* **2016**, *120*, 7101−7111.

(7) Akwi, F. M.; Watts, P. The in situ generation and reactive quench of diazonium compounds in the synthesis of azo compounds in microreactors. *Beilstein J. Org. Chem.* **2016**, *12*, 1987−2004.

(8) Patel, A. R.; Patel, G.; Maity, G.; Patel, S. P.; Bhattacharya, S.; Putta, A.; Banerjee, S. Direct oxidative azo coupling of anilines using a self-assembled flower-like $CuCo_2O_4$ material as a catalyst under aerobic conditions. *ACS Omega* **2020**, *5*, 30416−30424.

(9) Chen, W.; Li, H.; Jin, Y.; Wu, C.; Yuan, Z.; Ma, P.; Wang, J.; Niu, J. An intriguing tetranuclear Rh-based polyoxometalate for the reduction of nitroarene and oxidation of aniline. *Chem. Commun.* **2022**, *58*, 9902−9905.

(10) Liu, X.; Li, H. Q.; Ye, S.; Liu, Y. M.; He, H. Y.; Cao, Y. Gold-catalyzed direct hydrogenative coupling of nitroarenes to synthesize aromatic azo compounds. *Angew. Chem., Int. Ed.* **2014**, *53*, 7624−7628.

(11) Thorwirth, R.; Bernhardt, F.; Stolle, A.; Ondruschka, B.; Asghari, J. Switchable selectivity during oxidation of anilines in a ball mill. *Chem. - Eur. J.* **2010**, *16*, 13236−13242.

(12) Baer, E.; Tosoni, A. L. Formation of symmetric azo-compounds from primary aromatic amines by lead tetraacetate. *J. Am. Chem. Soc.* **1956**, *78*, 2857−2858.

(13) Zou, Y.; Zhang, M.; Cao, F.; Li, J.; Zhang, S.; Qu, Y. Single crystal MnOOH nanotubes for selective oxidative coupling of anilines to aromatic azo compounds. *J. Mater. Chem. A* **2021**, *9*, 19692−19697.

(14) Shabir, J.; Garkoti, C.; Gupta, P.; Sharma, M.; Rani, S.; Kumari, M.; Mozumdar, S. Ru_xPd_y alloy nanoparticles uniformly anchored on reduced graphene oxide nanosheets (Ru_xPd_y@rGO): A recyclable catalyst. *ACS Omega* **2021**, *6*, 1415−1425.

(15) Gao, B. B.; Zhang, M.; Chen, X. R.; Zhu, D. L.; Yu, H.; Zhang, W. H.; Lang, J. P. Preparation of carbon-based AuAg alloy nanoparticles by using the heterometallic $[Au_4Ag_4]$ cluster for efficient oxidative coupling of anilines. *Dalton Trans.* **2018**, *47*, 5780−5788.

(16) Cai, S.; Rong, H.; Yu, X.; Liu, X.; Wang, D.; He, W.; Li, Y. Room temperature activation of oxygen by monodispersed metal nanoparticles: Oxidative dehydrogenative coupling of anilines for azobenzene syntheses. *ACS Catal.* **2013**, *3*, 478−486.

(17) Kumar, M.; Soni, K.; Yadav, G. D.; Singh, S.; Deka, S. Surfactant directed $Ag_{1-x}Ni_x$ alloy nanoparticle catalysed synthesis of aromatic azo derivatives from aromatic amines. *Appl. Catal., A* **2016**, *525*, 50−58.

(18) Saha, A.; Payra, S.; Selvaratnam, B.; Bhattacharya, S.; Pal, S.; Koodali, R. T.; Banerjee, S. Hierarchical mesoporous RuO_2/Cu_2O nanoparticle-catalyzed oxidative homo/hetero azo-coupling of anilines. *ACS Sustainable Chem. Eng.* **2018**, *6*, 11345−11352.

(19) Wang, J.; He, J.; Zhi, C.; Luo, B.; Li, X.; Pan, Y.; Cao, X.; Gu, H. Highly efficient synthesis of azos catalyzed by the common metal copper (0) through oxidative coupling reactions. *RSC Adv.* **2014**, *4*, 16607−16611.

(20) Jiang, B.; Du, Y. Y.; Han, G. Z. Palladium-mediated base-free and solvent-free synthesis of aromatic azo compounds from anilines catalyzed by copper acetate. *Green Process. Synth.* **2022**, *11*, 823−829.

(21) Sitter, J. D.; Vannucci, A. K. Photocatalytic Oxidative Coupling of Arylamines for the Synthesis of Azoaromatics and the Role of O_2 in the Mechanism. *J. Am. Chem. Soc.* **2021**, *143*, 2938−2943.

(22) Zhu, P. Y.; Han, X.; Wang, X. M.; Liu, Y.; Wu, S. H.; Wang, S. J.; Xu, Z.; Jia, S. Y.; Ren, H. T. Selective oxidation of aniline contaminants via a hydrogen-abstraction pathway by $Bi_{2\cdot15}WO_6$ under visible light and alkaline conditions. *Chemosphere* **2020**, *261*, No. 127719.

(23) Chen, J.; Shen, C.; Guo, B.; Yu, Y.; Wu, L. Photocatalytic oxidation of aniline over MO/TiO_2 (M = Mg, Ca, Sr, Ba) under visible light irradiation. *Catal. Today* **2019**, *335*, 312−318.

(24) Singh, A. K.; Xu, Q. Synergistic catalysis over bimetallic alloy nanoparticles. *ChemCatChem* **2013**, *5*, 652−676.

(25) Sachi; Singh, A. P.; Thirumal, M. Fabrication of AgNi Nanoalloy-Decorated ZnO Nanocomposites as an Efficient and Novel Hybrid Catalyst to Degrade Noxious Organic Pollutants. *ACS Omega* **2021**, *6*, 34771−34782.

(26) Fang, H.; Yang, J.; Wen, M.; Wu, Q. Nanoalloy materials for chemical catalysis. *Adv. Mater.* **2018**, *30*, No. 1705698.

(27) Udayabhaskar, R.; Sreekanth, P.; Karthikeyan, B. Optical and nonlinear optical limiting properties of AgNi alloy nanostructures. *Plasmonics* **2016**, *11*, 1461−1466.

(28) Bhandary, N.; Singh, A. P.; Kumar, S.; Ingole, P. P.; Thakur, G. S.; Ganguli, A. K.; Basu, S. In situ solid-state synthesis of a AgNi/g-C_3N_4 nanocomposite for enhanced photoelectrochemical and photocatalytic activity. *ChemSusChem* **2016**, *9*, 2816−2823.

(29) Guo, J.; Wang, X.; Miao, P.; Liao, X.; Zhang, W.; Shi, B. One-step seeding growth of controllable Ag@Ni core−shell nanoparticles on skin collagen fiber with introduction of plant tannin and their application in high-performance microwave absorption. *J. Mater. Chem.* **2012**, *22*, 11933−11942.

(30) Gaudry, M.; Cottancin, E.; Pellarin, M.; Lermé, J.; Arnaud, L.; Huntzinger, J. R.; Vialle, J. L.; Broyer, M.; Rousset, J. L.; Treilleux, M.; Mélinon, P. Size and composition dependence in the optical properties of mixed (transition metal/noble metal) embedded clusters. *Phys. Rev. B* **2003**, *67*, No. 155409.

(31) Ma, E. Alloys created between immiscible elements. *Prog. Mater. Sci.* **2005**, *50*, 413−509.

(32) Zhang, Z.; Nenoff, T. M.; Leung, K.; Ferreira, S. R.; Huang, J. Y.; Berry, D. T.; Provencio, P. P.; Stumpf, R. Room-temperature synthesis of Ag− Ni and Pd− Ni alloy nanoparticles. *J. Phys. Chem. C* **2010**, *114*, 14309−14318.

(33) Majee, R.; Kumar, A.; Das, T.; Chakraborty, S.; Bhattacharyya, S. Tweaking nickel with minimal silver in a heterogeneous alloy of

decahedral geometry to deliver platinum-like hydrogen evolution activity. *Angew. Chem., Int. Ed.* **2020**, *59*, 2881−2889.
(34) Yan, S.; Sun, D.; Tan, Y.; Xing, X.; Yu, H.; Wu, Z. Synthesis and formation mechanism of Ag−Ni alloy nanoparticles at room temperature. *J. Phys. Chem. Solids* **2016**, *98*, 107−114.
(35) Kumar, M.; Deka, S. Multiply twinned AgNi alloy nanoparticles as highly active catalyst for multiple reduction and degradation reactions. *ACS Appl. Mater. Interfaces* **2014**, *6*, 16071−16081.
(36) Dhanda, R.; Kidwai, M. Reduced graphene oxide supported Ag_xNi_{100-x} alloy nanoparticles: a highly active and reusable catalyst for the reduction of nitroarenes. *J. Mater. Chem. A* **2015**, *3*, 19563−19574.
(37) Kumar, A.; Mathur, N. Photocatalytic oxidation of aniline using Ag^+-loaded TiO_2 suspensions. *Appl. Catal., A* **2004**, *275*, 189−197.

https://doi.org/10.1021/acsomega.2c07441
ACS Omega 2022, 7, 48615−48622